Turbo Processing for Scalar and Vector Channels

Stephan ten Brink and Gerhard Kramer
Bell Laboratories, 600 Mountain Ave, Murray Hill, NJ 07974, USA
E-mail: tenbrink@ieee.org, gkr@bell-labs.com

Abstract: *Repeat–accumulate codes are designed for scalar and vector channels by using a curve–fitting procedure on extrinsic information transfer (EXIT) charts. The scalar channel code designs are done for 8-ary phase shift keying (8–PSK) and different bit labelings. It is found that curve fitting can give capacity–approaching codes irrespective of the labeling. The vector channel (multi–input, multi–output or MIMO) code designs are done for two demodulator structures, namely an inner detection loop and a trellis detector. The trellis detector is shown to be more robust to system changes.*

Keywords: Turbo codes, repeat–accumulate codes, modulation, detection, mutual information.

1. Introduction

The discovery of capacity–approaching codes for erasure channels [1]–[2] has led to new code design techniques for other channels [3], [4]. For example, code design for erasure channels can be interpreted as a *curve–fitting* procedure on extrinsic information transfer (EXIT) charts [5]–[9]. The curve–fitting applies to other channels, and we continue the investigations of [7]–[8] on such generalizations.

We consider two problems. First, we study the applicability of EXIT curve–fitting to higher–order modulations, and in particular to 8-ary phase–shift keying (8–PSK) with different bit labelings. Second, we study the robustness of two types of demodulator structures for vector (multi–input, multi–output or MIMO) channels, namely an inner detection loop and a trellis detector. Our focus for both problems is on *modulation and detection*, so we perform all our designs with one class of codes, namely the *nonsystematic* repeat-accumulate (RA) codes introduced in [8]. Similar designs could also be done for other code families.

This paper is organized as follows. In Section 2. we show how to design RA codes used with binary phase shift keying (BPSK) on additive white Gaussian noise (AWGN) channels. Section 3. extends this approach to 8–PSK. In Section 4. we combine detection and decoding for MIMO fading channels. We further compare an inner detection loop and a trellis detector in terms of their robustness to system changes. Section 5. summarizes our findings.

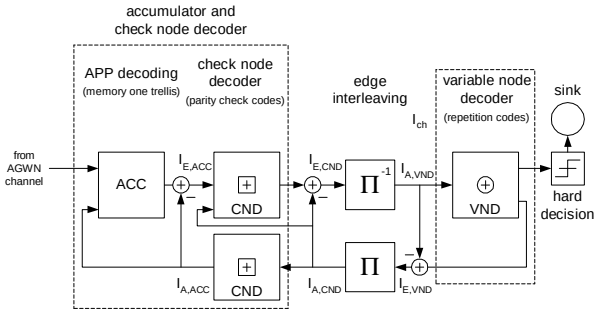

Figure 1: Decoder for a nonsystematic RA code.

2. Nonsystematic RA Codes

RA codes can operate near capacity for many channels, just like low–density parity–check (LDPC) codes [4], parallel concatenated (PC or turbo) [10] codes, and serially concatenated (SC) codes [11]. Two classes of irregular RA codes were introduced in [2]: systematic and nonsystematic. Both classes are *check–regular* in the sense that the encoder has a layer of check nodes where each check node takes as inputs exactly d_c edges from an interleaver. However, the check–regular, nonsystematic RA decoders require $d_c > 1$ to approach capacity, yet do not even begin to converge for such cases [2]. This problem is solved in [8] by making the check node layer *biregular*, i.e., the check nodes have either degree 1 or d_c. This trick is akin to *code doping* [12] and it enables a successful start to the iterative decoding. We consider only these check–biregular, nonsystematic RA codes from here on.

2.1. Code and Iterative Decoder

The encoder consists of four main parts: k repetition codes, an interleaver, n single parity check codes, and a differential encoder or *accumulator*. The repetition codes are represented as *variable nodes*, the interleaver as an edge interleaver, the single parity check codes as *check nodes*, and the accumulator as a chain of check nodes.

An iterative decoder is depicted in Fig. 1. The inner decoder takes the n channel reliability values

(log–likelihood ratio values or L–values [13]) for the parity bits and performs an *a posteriori* probability (APP) bit decoding over the memory–one trellis of the accumulator. The resulting output L–values are forwarded to the inner check node decoder (CND) comprising the n check nodes. The CND generates L–values that are forwarded to the outer variable node decoder (VND) comprising k variable nodes. The VND uses these L–values to generate new L–values that are fed back through the edge interleaver to the CND. Finally, one decoder iteration is completed when the CND generates L–values that it feeds back to the accumulator decoder (ACC). We will often consider the ACC and the CND as a single decoding unit that we refer to as the ACC&CND-decoder.

2.2. EXIT Curve of the Outer VND

We begin with the VND. A variable node of degree d_v has d_v incoming messages, and it decodes by adding L–values. The decoder outputs are

$$L_{i,out} = \sum_{j \neq i} L_{j,in} \tag{1}$$

where $L_{j,in}$ is the jth *a priori* L–value going into the variable node, and $L_{i,out}$ is the ith extrinsic L–value coming out of the variable node. We model $L_{j,in}$ as the output L–value of an AWGN channel whose input was the jth interleaver bit transmitted using BPSK. The EXIT function of a degree–d_v variable node is then (see [7, Sec. II])

$$I_{E,VND}(I_A, d_v) = J\left(\sqrt{(d_v - 1)} \cdot J^{-1}(I_A)\right). \tag{2}$$

where the functions $J(\cdot)$ and $J^{-1}(\cdot)$ are given in [7] and [14, eq. (15)].

Fig. 2 plots several VND curves, and we have included curves of systematic RA codes for comparison. For *nonsystematic* RA codes the EXIT curves (dashed lines) start at the origin. For the *systematic* RA codes the EXIT curves (solid lines) begin at positive values of $I_{E,VND}$ (the curves are computed for $E_b/N_0 = 0.5$dB and $R = 1/2$; L_{ch} is the "systematic" L–value coming from the channel whose variance is $8R\,E_b/N_0$).

2.3. EXIT Curve of the Inner CND

Consider next the CND. A check node of degree d_c has $d_c + 1$ incoming messages, d_c from the edge interleaver, and one from the accumulator. The decoding of a degree d_c check node is therefore the same as the decoding of a length $d_c + 1$ (or rate $d_c/(d_c + 1)$) single parity check code. The output L–values are (see [13, Sec. II.A])

$$L_{i,out} = \ln \frac{1 - \prod_{j \neq i} \frac{1 - e^{L_{j,in}}}{1 + e^{L_{j,in}}}}{1 + \prod_{j \neq i} \frac{1 - e^{L_{j,in}}}{1 + e^{L_{j,in}}}}. \tag{3}$$

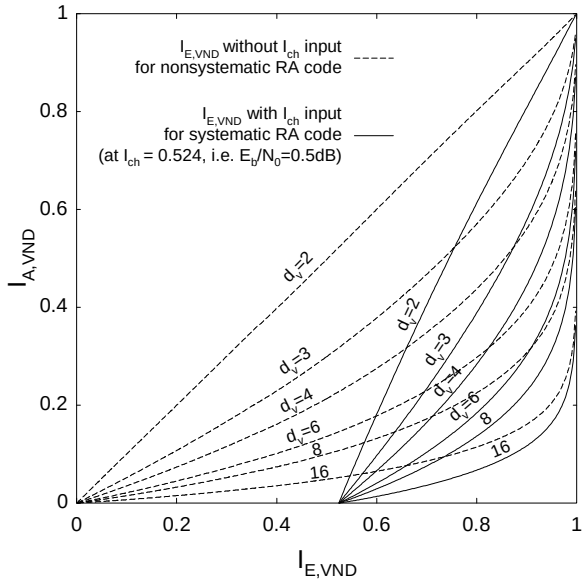

Figure 2: VND EXIT curves for nonsystematic (dashed lines) and systematic (solid lines) RA codes.

where the indices i and j include the d_c messages from the edge interleaver and the message from the accumulator. We again model $L_{j,in}$ as if one had transmitted the jth interleaver bit over an AWGN channel using BPSK.

For further analysis, we consider separately the two directions of information flow through the CND: 1) The *CND-to-ACC direction* where L–values are fed back from the interleaver to the ACC, and 2) the *CND-to-interleaver direction* where L–values are fed forward through the edge interleaver to the VND.

CND-to-ACC direction: We use a duality property for erasure channels that expresses the EXIT curve $I_{E,SPC}(\cdot)$ of the length d_c single parity check code in terms of the EXIT curve $I_{E,REP}(\cdot)$ of the length d_c repeat code (see [15, p. 189] and [6]). The result is

$$I_{E,SPC}(I_A, d_c) \approx 1 - I_{E,REP}\left(1 - I_A, d_c\right). \tag{4}$$

Simulations show this to be an accurate approximation, so we write the EXIT curve of the CND-to-ACC direction as

$$\begin{aligned} I_{A,ACC}(I_A, d_c) &\approx 1 - I_{E,REP}\left(1 - I_A, d_c + 1\right) \\ &= 1 - J\left(\sqrt{d_c} \cdot J^{-1}\left(1 - I_A\right)\right). \end{aligned} \tag{5}$$

CND-to-interleaver direction: Each CND node computes extrinsic information using its L–value from the ACC, and $d_c - 1$ L–values from the edge interleaver. We use a generalized duality result for erasure channels [9] and approximate the EXIT curve of the

CND-to-interleaver direction as

$$I_{E,CND}\left(I_A, I_E, d_c\right) \approx 1 - I_{E,REP}\left(1 - I_A, 1 - I_E, d_c\right)$$
$$= 1 - J\left(\sqrt{\left(d_c - 1\right)\left[J^{-1}\left(1 - I_A\right)\right]^2 + \left[J^{-1}\left(1 - I_E\right)\right]^2}\right) \quad (6)$$

where $I_A = I_{A,CND}$ and $I_E = I_{E,ACC}$.

2.4. EXIT Curve of the Inner ACC

We compute the EXIT function of the accumulator decoder (a unit memory trellis decoder) by simulation and denote it by

$$I_{E,ACC}(I_{A,ACC}, E_b/N_0, R). \quad (7)$$

We point out that the purpose of the accumulator is to make $I_E(I_A = 1) = 1$, i.e., without the accumulator the check node layer will have $I_E(I_A = 1) < 1$.

2.5. EXIT Curve of the Combined Inner ACC and CND

We combine (5)–(7) to approximate the transfer curve $I_{E,ACC\&CND}$ of the inner decoder comprising the ACC and CND. The result is

$$I_{E,ACC\&CND}\left(I_{A,CND}, d_c, E_b/N_0, R\right)$$
$$= I_{E,CND}\left(I_{A,CND}, I_{E,ACC}(I_{A,ACC}, E_b/N_0, R), d_c\right)$$
$$= I_{E,CND}\left(I_{A,CND},\right.$$
$$\left. I_{E,ACC}\left(I_{A,ACC}\left(I_{A,CND}, d_c\right), E_b/N_0, R\right), d_c\right). \quad (8)$$

Fig. 3 depicts several such curves. Note that the ACC curve is recovered by setting $d_c = 1$.

Observe that the curves with $d_c > 1$ in Fig. 3 and the nonsystematic VND curves in Fig. 2 start at the origin. This means that the decoder cannot even begin to converge which led [2] to remark that nonsystematic RA codes are useless for $d_c > 1$. This problem is solved in [8] by using a check node layer that is *biregular*, i.e., a non–zero fraction $a_{c,1}$ of the check nodes have degree $d_{c,1} = 1$.

We also remark that rather than measuring $I_{E,ACC}$ and computing $I_{E,ACC\&CND}$ via (8) one can alternatively measure $I_{E,ACC\&CND}$ directly. This approach is practical because the latter curve does not change for the curve fitting procedure described next.

2.6. EXIT Curves for Code Mixtures

Let $D_c = 2$ be the number of different check node degrees, and denote these by $\widetilde{d}_{c,1} = 1$ and $\widetilde{d}_{c,2}$. We compute the average check node degree as

$$\overline{d}_c = \sum_{i=1}^{D_c} a_{c,i} \cdot \widetilde{d}_{c,i} = a_{c,1} + a_{c,2} \cdot \widetilde{d}_{c,2} \quad (9)$$

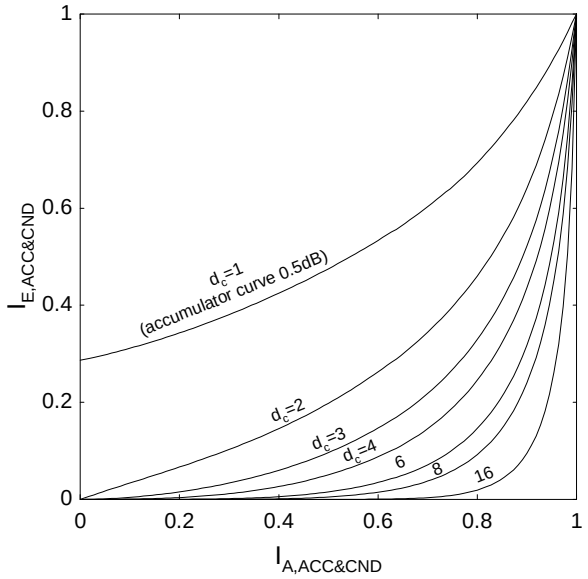

Figure 3: EXIT curves for the ACC and CND. AWGN channel with $E_b/N_0 = 0.5$dB at $R = 1/2$.

where $a_{c,i}$ is the fraction of check nodes with degree $\widetilde{d}_{c,i}$. Let $b_{c,i}$ be the fraction of *edges* incident to check nodes having degree $\widetilde{d}_{c,i}$. In [6], [16] it is shown that the EXIT curve of a mixture of codes is an average of the component EXIT curves. As in [7], we must average using the $b_{c,i}$ (and not the $a_{c,i}$) because it is the *edges* that carry the extrinsic messages. The EXIT curve of the ACC and biregular CND is therefore

$$I_{E,ACC\&CND}(I_A)$$
$$= \sum_{i=1}^{2} b_{c,i} \cdot I_{E,ACC\&CND}(I_A, \widetilde{d}_{c,i}, E_b/N_0, R). \quad (10)$$

Alternatively, one can estimate this EXIT curve by Monte–Carlo simulation [5]. Fig. 4 plots several such EXIT curves. Observe that $a_{c,1} > 0$ makes the curves start above the origin. This will initiate convergence when the ACC and CND are combined with a VND.

Let D_v be the number of different variable node degrees, and denote these by $\widetilde{d}_{v,i}$, $i = 1, \ldots, D_v$. We write the average variable node degree as

$$\overline{d}_v = \sum_{i=1}^{D_v} a_{v,i} \cdot \widetilde{d}_{v,i} \quad (11)$$

where $a_{v,i}$ is the fraction of variable nodes having degree $\widetilde{d}_{v,i}$. Let $b_{v,i}$ be the fraction of *edges* incident to variable nodes having degree $\widetilde{d}_{v,i}$. The VND transfer curve is therefore

$$I_{E,VND}\left(I_A\right) = \sum_{i=1}^{D_v} b_{v,i} \cdot I_{E,VND}\left(I_A, \widetilde{d}_{v,i}\right). \quad (12)$$

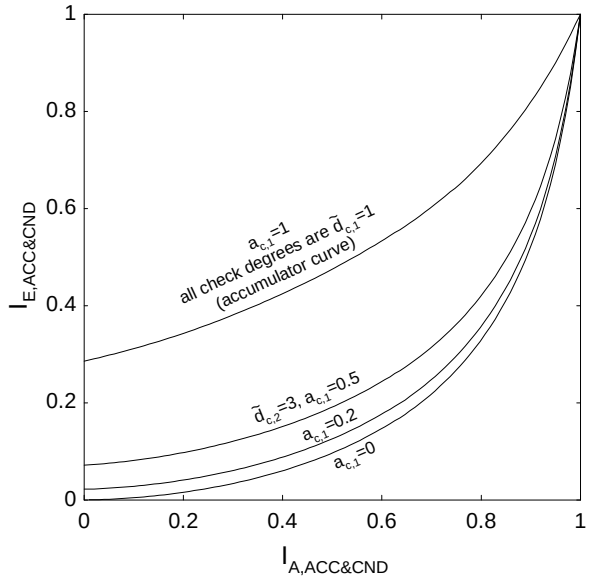

Figure 4: EXIT curves for an ACC and a biregular CND. The AWGN channel has $E_b/N_0 = 0.5$dB at a code rate of $R = 1/2$.

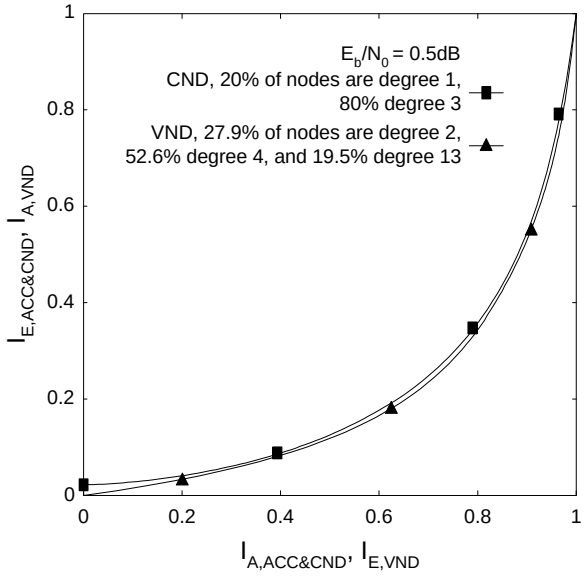

Figure 5: Design example of a nonsystematic RA code with $R = 1/2$.

The number of interleaver edges is $k\,\overline{d}_v = n\,\overline{d}_c$ so that

$$\overline{d}_v = \overline{d}_c\,/R\,. \tag{13}$$

Note that only $D_v - 2$ of the $\widetilde{d}_{v,i}$ can be adjusted freely because we must enforce (13) and $\sum_i b_{v,i} = 1$. Thus, we must choose $D_v \geq 3$ to permit curve fitting.

2.7. Design Example

We proceed by fitting the EXIT curve of the VND to that of the ACC&CND. We consider $R = 1/2$ and BPSK modulation on AWGN channels. The E_b/N_0 capacity limit for this setup is at 0.19dB. We choose $D_v = 3$ and perform the curve fitting at 0.5dB. Choosing $D_v > 3$ would let us approach capacity even more closely.

Fig. 5 shows a curve fit for a *nonsystematic* RA code with a *biregular* CND layer. The code's parameters are $a_{c,1} = 0.2$, $\widetilde{d}_{c,1} = 1$, $\widetilde{d}_{c,2} = 3$ and

$$\begin{array}{lll} \widetilde{d}_{v,1} = 2, & a_{v,1} = 0.2789, & b_{v,1} = 0.1073, \\ \widetilde{d}_{v,2} = 4, & a_{v,2} = 0.5258, & b_{v,2} = 0.4044, \\ \widetilde{d}_{v,3} = 13, & a_{v,3} = 0.1953, & b_{v,3} = 0.4883. \end{array}$$

The code has a convergence threshold at about 0.5dB. Furthermore, simulations with length $n = 10^5$ codes and 100 iterations show a turbo cliff at about 0.5dB (we measure the turbo cliff at a bit error rate (BER) of 10^{-4}). We remark that the usual error "floor" was observed near a BER of 10^{-5}. The error floor could be lowered by increasing the variable and check node degrees, but this also increases the number of edges and hence the decoding complexity.

3. RA Codes and Scalar Detection

Consider the system depicted in Fig. 6, and suppose we use the scalar AWGN channel. Suppose further that we use 8–PSK with one of the two labelings shown in Fig. 7. The labeling on the left is the Gray–mapping and we refer to the second labeling as D23. We combine an 8–PSK detector with the inner decoder (comprising the ACC and a check–biregular CND layer) of a nonsystematic RA code to form a new inner decoder. We further design the VND transfer curve to match the compound inner detector/ACC/CND transfer curve.

3.1. EXIT Curve of the Detector

The 8–PSK detector performs APP bit detection by considering all 8 hypotheses on the transmitted symbol. The detector EXIT curve cannot be described in closed form so we measure it by Monte–Carlo simulation. We denote the detector by DET and its EXIT curve by

$$I_{E,DET}\left(I_{A,DET}, E_b/N_0, R\right) \tag{14}$$

where R is the code rate (the overall rate is therefore $3R$ bits/use). The curves for the two labelings of Fig. 7 are plotted on the left of Fig. 8. Observe that the D23 labeling curve has a steep slope, whereas the Gray–labeling curve hardly changes with $I_{A,DET}$.

3.2. EXIT Curve of the Combined Detector, ACC and CND

We connect the 8–PSK detector to the inner RA decoder via the interleaver Π_2 as shown in Fig. 6.

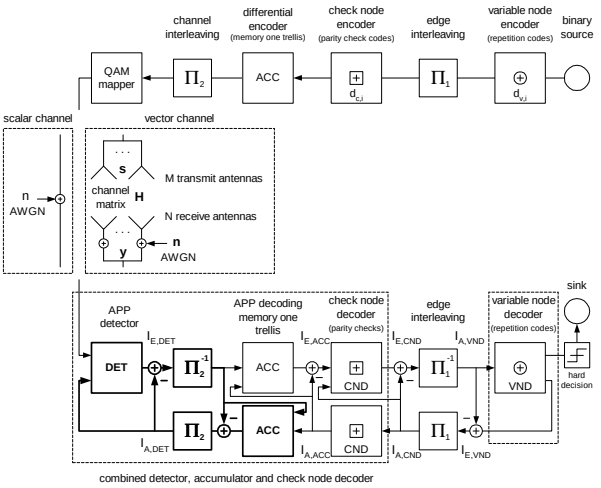

Figure 6: System model.

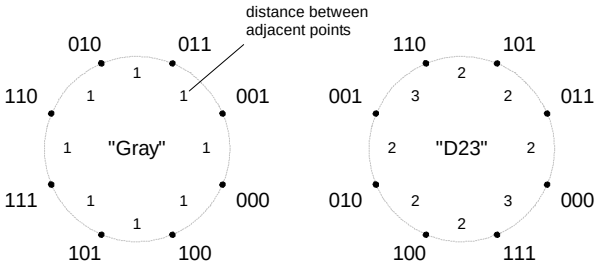

Figure 7: Two 8–PSK labelings.

The receiver chain of Fig. 6 is thus a double serial concatenation (see [20]). Such a structure requires an *inner detection loop*, i.e., iterations between the detector and the ACC (shown as thick lines in Fig. 6). We found that three to four iterations suffice. For example, the right of Fig. 8 shows the combined DET, ACC and CND curves after different numbers of inner iterations for the D23 labeling. We achieve saturation after three iterations. As in this figure, we denote the overall transfer curve of the inner decoder as $I_{E,D\&A\&C}(I_{A,D\&A\&C})$, or simply as $I_{E,CND}(I_{A,CND})$.

3.3. Design Examples

We set $R = 1/2$ and perform curve–fittings for both the Gray and D23 labelings. The Gray labeling parameters are $a_{c,1} = 0.2, \widetilde{d}_{c,1} = 1, \widetilde{d}_{c,2} = 3$, and

$$\begin{array}{lll} \widetilde{d}_{v,1} = 2, & a_{v,1} = 0.2710, & b_{v,1} = 0.1042, \\ \widetilde{d}_{v,2} = 4, & a_{v,2} = 0.5548, & b_{v,2} = 0.4268, \\ \widetilde{d}_{v,3} = 14, & a_{v,3} = 0.1742, & b_{v,3} = 0.4690. \end{array}$$

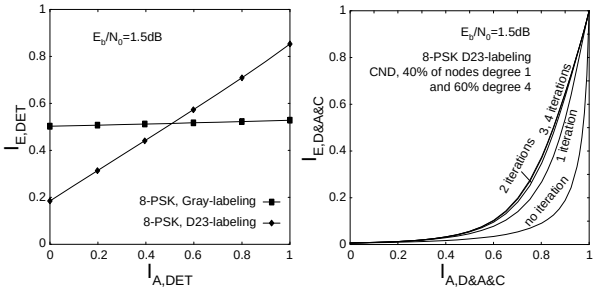

Figure 8: Left: 8–PSK detector EXIT curves. Right: combined detector (D23 labeling), ACC and CND transfer curve after several inner DET/ACC iterations. Parameters: $R = 1/2$, $E_b/N_0 = 0.5$dB, $n = 120\,000$, $a_{c,1} = 0.4$, $\widetilde{d}_{c,1} = 1$, $\widetilde{d}_{c,2} = 4$.

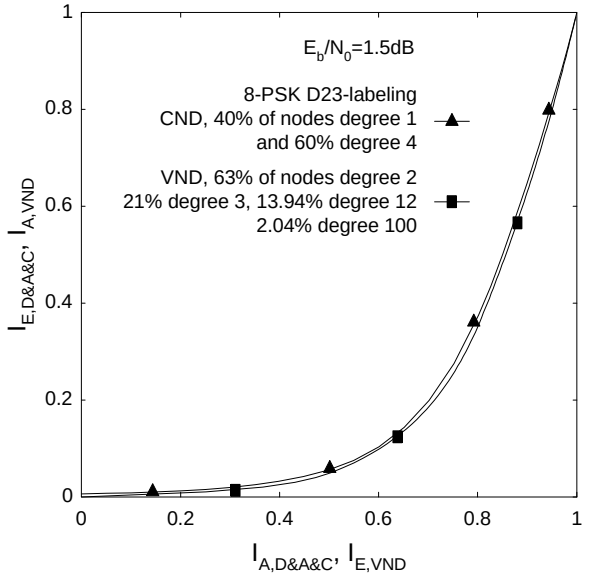

Figure 9: Design example for the D23–labeling (4 inner DET/ACC iterations).

The D23 labeling parameters are $a_{c,1} = 0.4, \widetilde{d}_{c,1} = 1, \widetilde{d}_{c,2} = 4$, and

$$\begin{array}{lll} \widetilde{d}_{v,1} = 2, & a_{v,1} = 0.6302, & b_{v,1} = 0.2251, \\ \widetilde{d}_{v,2} = 3, & a_{v,2} = 0.2101, & b_{v,2} = 0.1125, \\ \widetilde{d}_{v,3} = 12, & a_{v,3} = 0.1394, & b_{v,3} = 0.2987, \\ \widetilde{d}_{v,4} = 100, & a_{v,4} = 0.0204, & b_{v,4} = 0.3637. \end{array}$$

Fig. 9 plots the resulting EXIT chart for the D23 curve fit at $E_b/N_0 = 1.5$dB (capacity is at 1.27dB for an overall rate of 3/2 bits/use).

We next simulated to verify the designs. The simulation parameters were: code length $n = 120\,000$, random interleaver, 200 decoder iterations. The Gray labeling turbo cliff (BER of 10^{-4}) is at about 1.6dB. The D23 labeling turbo cliff is at about 1.8dB. In other words, *we can approach capacity for either la-*

beling by performing appropriate curve–fits. The price paid for using the D23 labeling is that the inner EXIT curve is steep. Thus, we have to use more variable node degrees for our curve–fitting. Also, the D23 labeling had a higher error "floor" because we used more degree two nodes.

4. RA Codes and Vector Detection

Consider next the system of Fig. 6 but with a vector channel having M transmit and N receive antennas. Each transmitter symbol is an $M \times 1$ vector $\mathbf{s} = [s_1, ..., s_M]^T$ whose entries take on complex values in a constellation set. We consider constellations of size 2^{M_c} so that each symbol carries $M \cdot M_c$ coded bits. For example, for 8–PSK we have $M_c = 3$. The average energy per transmit symbol is limited to E_s, and we assume that $E[||s_m||^2] = E_s/M$.

The receiver sees $N \times 1$ vectors $\mathbf{y} = \mathbf{H}\mathbf{s} + \mathbf{n}$ where $\mathbf{H}$ is the $N \times M$ channel matrix and $\mathbf{n}$ is a $N \times 1$ noise vector. We assume the entries of $\mathbf{n}$ to be independent, complex, zero–mean, Gaussian random variables with independent real and imaginary parts each having variance $\sigma^2 = N_0/2$. We define the normalized signal–to–noise ratio E_b/N_0 as

$$\left.\frac{E_b}{N_0}\right|_{\text{dB}} = \left.\frac{E_s}{N_0}\right|_{\text{dB}} + 10\log_{10}\frac{N}{RMM_c}. \qquad (15)$$

We assume $\mathbf{H}$ to be known by the receiver only, and consider a Rayleigh fading channel so that the entries of $\mathbf{H}$ are independent, complex, zero–mean, Gaussian random variables with independent real and imaginary parts each having variance $1/2$ [18, Sec. 4]. For a *quasistatic* channel the matrix $\mathbf{H}$ remains unchanged over long time intervals, while for an *ergodic* channel $\mathbf{H}$ changes for every symbol $\mathbf{s}$. We consider only the ergodic model whose capacity is (see [17]–[19])

$$C = E\left[\log_2 \det\left(\mathbf{I} + \frac{E_s}{N_0}\frac{1}{M}\mathbf{H}\mathbf{H}^\dagger\right)\right] \qquad (16)$$

where $\mathbf{I}$ is the identity matrix and $\mathbf{H}^\dagger$ denotes the complex–conjugate transpose of $\mathbf{H}$. One achieves capacity by using Gaussian distributed symbols $\mathbf{s}$. However, in this section we consider only quadrature phase shift keying (QPSK) with Gray labeling.

4.1. Trellis Detection

The receiver chain of Fig. 6 is again a double serial concatenation. An alternative to the structure of Fig. 6 is to omit the interleaver Π_2, as depicted in Fig. 10. The MIMO detection and accumulator decoding is now performed in a single trellis (see Fig. 11). This trellis has two states and 2^{MM_c} incoming/outgoing edges per state, each edge being labeled by the MM_c bits corresponding to one vector–channel symbol. The transition from one state to the

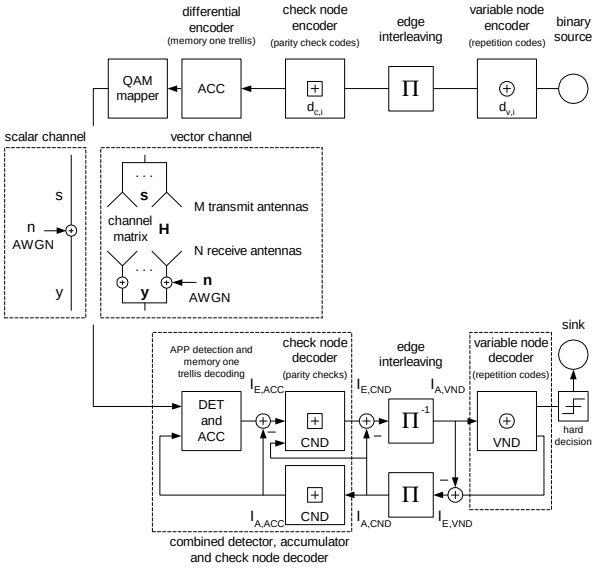

Figure 10: System model with trellis detection.

next is determined by running MM_c bits through the differential encoder, with 2^{MM_c-1} transitions arriving in state 0, and 2^{MM_c-1} transitions arriving in state 1. For detection/decoding, one can apply the Bahl, Cocke, Jelinek, Raviv (BCJR) algorithm [21] to the trellis.

The code design for this system is the same as above. However, the *trellis detection* has two advantages over the system of Fig. 6. First, no inner iterations are required which reduces decoding complexity; observe that the MIMO detector must perform the same APP bit detection for either scheme. Second, trellis detection is more robust against code parameter mismatches, as explained below.

4.2. Robustness

The detector EXIT curve depends mainly on the number of transmit and receive antennas. For example, a 4×4–MIMO detector does not benefit much from *a priori* knowledge, i.e., the EXIT curve is rather flat and close to the horizontal line of a 1×1–detector (see Fig. 12). In contrast, any detector with M much larger that N (e.g., a 4×1–MIMO detector) benefits substantially from *a priori* knowledge, resulting in an EXIT curve with a steep slope.

The detector behavior affects the EXIT curve of the combined MIMO detector (DET), accumulator decoder (ACC) and check node decoder (CND), which we abbreviate as D&A&C. The left of Fig. 13 shows such EXIT curves for different M and N when an *inner detection loop* is used. Observe that the 4×4–curve differs significantly from the 4×1 curve. The right of Fig. 13 shows the corresponding EXIT curves for *trellis detection*. Observe that the curves are now closer to each other than for the inner detection loop.

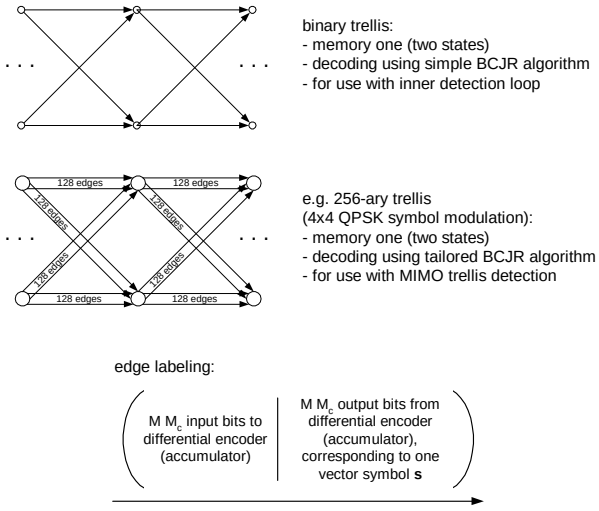

Figure 11: ACC trellis sections without (binary trellis) and with (2^{MM_c}–ary trellis) trellis detection.

Recall next that code design reduces to matching the outer VND curve to the inner D&A&C–curve. This means that if several inner curves are similar, an outer curve designed for one of them will perform reasonably well for all of them. This suggests that code parameter mismatches will affect systems using trellis detection less than those using an inner detection loop.

We perform the following experiment to verify this prediction. We design an RA code for an AWGN channel but use it for all the MIMO channels. Of course, there will be performance penalties because the code is not matched to the detectors individually, cf. [7], [8]. Fig. 14 plots the simulation results. Observe that the performance penalty is small for 4×4–channels, but is significant for 4×1–channels. Observe further that trellis detection suffers much less from code parameter mismatches than an inner detection loop. This means trellis detection is more forgiving if a channel varies faster than the time needed to adjust the code parameters. Thus, we say that trellis detection is *more robust against code parameter mismatches*. We remark that the above conclusions will also hold for any code rate, any number of transmit antennas, and many other channel models, e.g., quasistatic channels. Furthermore, adding an accumulator to other codes, e.g., LDPC codes, might also convey robustness to their decoders when used with trellis detection.

5. Summary

We demonstrated the applicability of EXIT curve–fitting to 8–PSK with two different labelings. Close–to–capacity performance can be achieved for many other mappings and modulations. We further showed

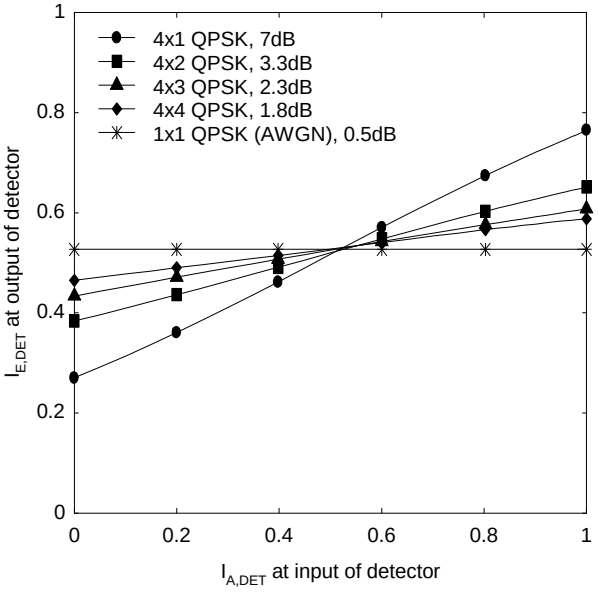

Figure 12: MIMO detector EXIT curves. E_b/N_0 is chosen so that the information rate across the channel is constant; code rate $R = 1/2$.

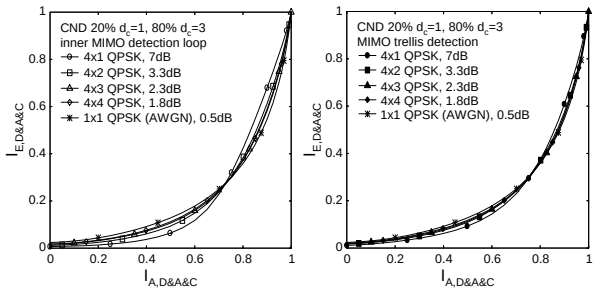

Figure 13: Left: EXIT curves of the D&A&C with an inner detection loop after 4 iterations. Right: trellis detection.

that trellis detection is more robust to system changes than an inner detection loop for MIMO channels.

REFERENCES

[1] M.G. Luby, M. Mitzenmacher, M.A. Shokrollahi, D.A. Spielman, and V. Stemann, "Practical Loss-Resilient Codes," in *Proc. 29th Annu. ACM Symp. Theory of Computing,* 1997, pp. 150-159.

[2] H. Jin, A. Khandekar, and R. McEliece, "Irregular repeat–accumulate codes," *Proc. 2nd Int. Conf. on Turbo Codes and Related Topics*, Brest, France, pp. 1–8, Sept. 2000.

[3] T. J. Richardson and R. L. Urbanke, "The capacity of low–density parity–check codes under message–passing decoding," *IEEE Trans. In-*

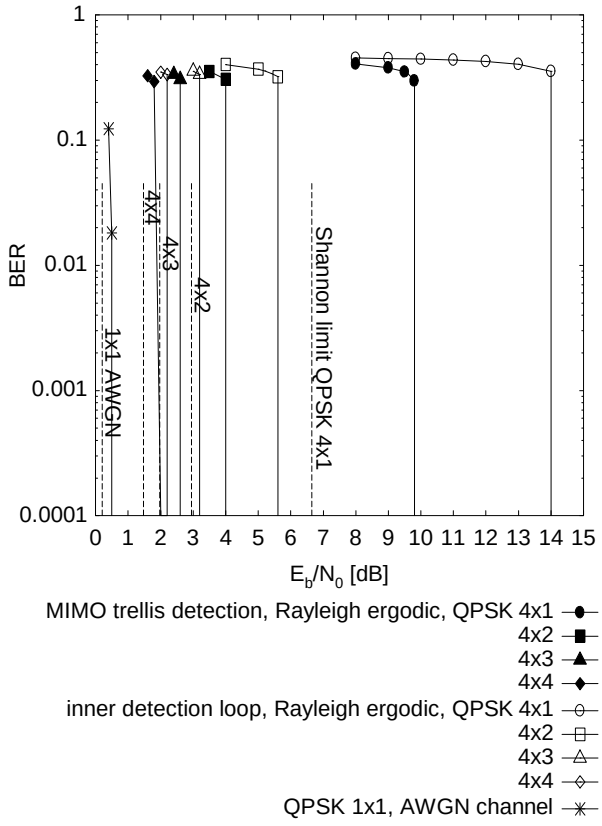

Figure 14: BER chart for various MIMO channels.

form. Theory, vol. 47, no. 2, pp. 599–618, Feb. 2001.

[4] T. J. Richardson, A. Shokrollahi, and R. L. Urbanke, "Design of capacity–approaching low–density parity–check codes," *IEEE Trans. Inform. Theory*, vol. 47, no. 2, pp. 619–637, Feb. 2001.

[5] S. ten Brink, "Convergence of iterative decoding," *Electron. Lett.*, vol. 35, no. 10, pp. 806–808, May 1999.

[6] A. Ashikhmin, G. Kramer, and S. ten Brink, "Extrinsic information transfer functions: A model and two properties," *36th Ann. Conf. on Inf. Sci. and Syst.*, Princeton, Mar. 2002.

[7] S. ten Brink, G. Kramer, and A. Ashikhmin, "Design of low–density parity–check codes for modulation and detection," submitted to *IEEE Trans. Commun.*, June 2002. Available at http://cm.bell-labs.com/who/gkr/pub.html.

[8] S. ten Brink and G. Kramer, "Design of repeat–accumulate codes for iterative detection and decoding," to appear in *IEEE Trans. Signal Proc.*, 2003. Available at http://cm.bell-labs.com/who/gkr/pub.html.

[9] A. Ashikhmin, G. Kramer, and S. ten Brink, "Extrinsic information transfer functions: model and erasure channel properties," submitted to the *IEEE Trans. Inform. Theory*, March 2003. Available at http://cm.bell-labs.com/who/gkr/pub.html.

[10] C. Berrou, A. Glavieux, and P. Thitimajshima, "Near Shannon limit error–correcting coding and decoding: Turbo–codes," *Proc. ICC*, pp. 1064–1070, May 1993.

[11] S. Benedetto, D. Divsalar, G. Montorsi, and F. Pollara, "Serial concatenation of interleaved codes: performance analysis, design, and iterative decoding," *IEEE Trans. Inform. Theory*, vol. 44, no. 3, pp. 909–926, May 1998.

[12] S. ten Brink, "Code doping for triggering iterative decoding convergence," *Proc. IEEE Int. Symp. Inform. Th.*, p. 235, July 2001.

[13] J. Hagenauer, E. Offer, and L. Papke, "Iterative decoding of binary block and convolutional codes," *IEEE Trans. Inform. Theory*, vol. 42, no. 2, pp. 429–445, Mar. 1996.

[14] S. ten Brink, "Convergence behavior of iteratively decoded parallel concatenated codes," *IEEE Trans. Commun.*, vol. 49, no. 10, pp. 1727–1737, Oct. 2001.

[15] S. Y. Chung, *On the construction of some capacity-approaching coding schemes,* Ph.D. Thesis, M.I.T., Cambridge MA, USA, Sept. 2000.

[16] M. Tuechler and J. Hagenauer, "EXIT charts and irregular codes," *36th Ann. Conf. on Inf. Sci. and Syst.*, Princeton, Mar. 2002.

[17] G. J. Foschini, "Layered space–time architecture for wireless communication in a fading environment when using multi–element antennas," *Bell Labs. Tech. J.*, vol. 1, no. 2, pp. 41–59, 1996.

[18] I. E. Telatar, "Capacity of multi–antenna Gaussian channels," *Eur. Trans. Telecom.*, vol. 10, pp. 585–595, Nov. 1999.

[19] E. Biglieri, J. Proakis, and S. Shamai (Shitz), "Fading channels: information-theoretic and communications aspects," *IEEE Trans. Inform. Theory*, vol. 44, no. 2, pp. 2619–2692, Oct. 1998.

[20] S. Benedetto, D. Divsalar, G. Montorsi, and F. Pollara, "Analysis, design, and iterative decoding of double serially concatenated codes with interleavers," *IEEE J. Sel. Areas Commun.*, vol 16, pp. 231–244, Feb. 1998.

[21] L. Bahl, J. Cocke, F. Jelinek, and J. Raviv, "Optimal decoding of linear codes for minimizing symbol error rate," *IEEE Trans. Inform. Theory*, vol. 20, pp. 284–287, Mar. 1974